Research Article | Vol. 25, No. 14 | 10 Jul 2017 | OPTICS EXPRESS 16347
Optics EXPRESS

Comparison of single-/few-/multi-mode 850 nm VCSELs for optical OFDM transmission

HSUAN-YUN KAO,[1] CHENG-TING TSAI,[1] SHAN-FONG LEONG,[1] CHUN-YEN PENG,[1] YU-CHIEH CHI,[1] JIAN JANG HUANG,[1] HAO-CHUNG KUO,[2] TIEN-TSORNG SHIH,[3] JAU-JI JOU,[3] WOOD-HI CHENG,[4] CHAO-HSIN WU,[1] AND GONG-RU LIN[1,*]

[1]*Graduate Institute of Photonics and Optoelectronics, and Department of Electrical Engineering, National Taiwan University, No. 1, Roosevelt Rd, Sect. 4, Taipei 10617, Taiwan*
[2]*Graduate Institute of Electro-Optical Engineering, and Department of Photonics, National Chiao Tung University, No. 1001, University Rd, Hsinchu 30100, Taiwan*
[3]*Department of Electronic Engineering, National Kaohsiung University of Applied Sciences, No. 415, Chien Kung Rd, Sanmin District, Kaohsiung 80778, Taiwan*
[4]*Graduate Institute of Optoelectronic Engineering, and Department of Electrical Engineering, National Chung Hsing University, No. 250, Kuo Kuang Rd, Taichung 402, Taiwan*
[*]*grlin@ntu.edu.tw*

For high-speed optical OFDM transmission applications, a comprehensive comparison of the homemade multi-/few-/single-transverse mode (MM/FM/SM) vertical cavity surface emitting laser (VCSEL) chips is performed. With microwave probe, the direct encoding of pre-leveled 16-QAM OFDM data and transmission over 100-m-long OM4 multi-mode-fiber (MMF) are demonstrated for intra-datacenter applications. The MM VCSEL chip with the largest emission aperture of 11 μm reveals the highest differential quantum efficiency which provides the highest optical power of 8.67 mW but exhibits the lowest encodable bandwidth of 21 GHz. In contrast, the SM VCSEL chip fabricated with the smallest emission aperture of only 3 μm provides the highest 3-dB encoding bandwidth up to 23 GHz at a cost of slight heat accumulation. After optimization, with the trade-off set between the receiving signal-to-noise ratio (SNR) and bandwidth, the FM VCSEL chip guarantees the highest optical OFDM transmission bit rate of 96 Gbit/s under back-to-back case with its strongest throughput. Among three VCSEL chips, the SM VCSEL chip with nearly modal-dispersion free feature is treated as the best candidate for carrying the pre-leveled 16-QAM OFDM data over 100-m OM4-MMF with same material structure but exhibits different oxide-layer confined gain cross-sections with one another at 80-Gbit/s with the smallest receiving power penalty of 1.77 dB.

OCIS codes: (140.7260) Vertical cavity surface emitting lasers; (060.2390) Fiber optics, infrared; (200.4650) Optical interconnects.

References and links

1. R. Safaisini, E. Haglund, A. Larsson, J. S. Gustavsson, E. P. Haglund, and P. Westbergh, "High-speed 850 nm VCSELs operating error free up to 57 Gbit/s," Electron. Lett. **49**(16), 1021–1023 (2013).
2. "IEEE P802.3bs 400 Gb/s Ethernet task force," (2016). *http://www.ieee802.org/3/bs/*
3. D. J. Law, W. W. Diab, A. Healey, S. B. Carlson, and V. Maguire, "IEEE 802.3 industry connections Ethernet bandwidth assessment," (IEEE 802.3 Industry Connections Bandwidth Assessment, 2012). *http://www.ieee802.org/3/ad_hoc/bwa/BWA_Report.pdf*
4. P. Westbergh, J. S. Gustavsson, Å. Haglund, M. Skold, A. Joel, and A. Larsson, "High-speed, low-current-density 850 nm VCSELs," IEEE J. Sel. Top. Quantum Electron. **15**(3), 694–703 (2009).
5. P. Westbergh, J. S. Gustavsson, B. Kögel, Å. Haglund, A. Larsson, A. Mutig, A. Nadtochiy, D. Bimberg, and A. Joel, "40 Gbit/s error-free operation of oxide-confined 850 nm VCSEL," Electron. Lett. **46**(14), 1014–1016 (2010).
6. C.-T. Tsai, S. Chang, C.-Y. Pong, S.-F. Liang, Y.-C. Chi, C.-H. Wu, T.-T. Shih, J. J. Huang, H.-C. Kuo, W.-H. Cheng, and G.-R. Lin, "RIN suppressed multimode 850-nm VCSEL for 56-Gbps 16-QAM OFDM and 22-Gbps

#294917 https://doi.org/10.1364/OE.25.016347
Journal © 2017 Received 1 May 2017; revised 10 Jun 2017; accepted 10 Jun 2017; published 30 Jun 2017

Optics EXPRESS

PAM-4 transmission," in *Conference on Optical Fiber Communication* (Anaheim, CA, USA, 2016), paper Th4D.2.
7. H. E. Li and K. Iga, *Vertical-Cavity Surface-Emitting Laser Devices* (Springer, 2003).
8. D. M. Kuchta, A. V. Rylyakov, C. L. Schow, J. E. Proesel, C. Baks, P. Westbergh, J. S. Gustavsson, and A. Larsson, "64Gb/s transmission over 57m MMF using an NRZ modulated 850nm VCSEL," in *Conference on Optical Fiber Communication* (San Francisco, CA, USA, 2014), paper Th3C. 2.
9. B. Kögel, J. S. Gustavsson, E. Haglund, R. Safaisini, A. Joel, P. Westbergh, M. Geen, R. Lawrence, and A. Larsson, "High-speed 850 nm VCSELs with 28 GHz modulation bandwidth operating error-up to 44 Gbit/s," Electron. Lett. **48**(18), 1145–1147 (2012).
10. A. Gholami, D. Molin, and P. Sillard, "Compensation of chromatic dispersion by modal dispersion in MMF- and VCSEL-based gigabit Ethernet transmissions," IEEE Photonics Technol. Lett. **21**(10), 645–647 (2009).
11. R. Safaisini, K. Szczerba, P. Westbergh, E. Haglund, B. Kögel, J. S. Gustavsson, M. Karlsson, P. Andrekson, and A. Larsson, "High-speed 850 nm quasi-single-mode VCSELs for extended-reach optical interconnects," J. Opt. Commun. Netw. **5**(7), 686–695 (2013).
12. K. Szczerba, P. Westbergh, J. Karout, J. S. Gustavsson, Å. Haglund, M. Karlsson, P. A. Andrekson, E. Agrell, and A. Larsson, "4-PAM for high-speed short-range optical communications," J. Opt. Commun. Netw. **4**(11), 885–894 (2012).
13. M. Jungo, F. M. Di Sopra, D. Erni, and W. Baechtold, "Scaling effects on vertical-cavity surface-emitting lasers static and dynamic behavior," Appl. Phys. Lett. **91**(9), 5550–5557 (2002).
14. P. Moser, P. Wolf, G. Larisch, H. Li, J. A. Lott, and D. Bimberg, "Energy-efficient oxide-confined high-speed VCSELs for optical interconnects," Proc. SPIE **9001**, 1–8 (2014).
15. P. Moser, J. A. Lott, P. Wolf, G. Larisch, H. Li, N. Ledentsov, and D. Bimberg, "Impact of the aperture diameter on the energy efficiency of oxide-confined 850 nm high speed VCSELs," Proc. SPIE **8639**, 86390V (2013).
16. Å. Haglund, J. S. Gustavsson, J. Vukusic, P. Modh, and A. Larsson, "Single fundamental-mode output power exceeding 6 mW from VCSELs with a shallow surface relief," IEEE Photonics Technol. Lett. **16**(2), 368–370 (2004).
17. M. P. Tan, S. T. M. Fryslie, J. A. Lott, N. N. Ledentsov, D. Bimberg, and K. D. Choquette, "Error-free transmission over 1-km OM4 multimode fiber at 25 Gb/s using a single mode photonic crystal vertical-cavity surface-emitting laser," IEEE Photonics Technol. Lett. **25**(18), 1823–1825 (2013).
18. P. Westbergh, A. Larsson, E. Haglund, R. Safaisini, and J. S. Gustavsson, "20 Gbit/s data transmission over 2 km multimode fibre using 850 nm mode filter VCSEL," Electron. Lett. **50**(1), 40–42 (2014).
19. R. Michalzik and K. J. Ebeling, "Generalized BV diagrams for higher order transverse modes in planar vertical-cavity laser diodes," IEEE J. Quantum Electron. **31**(8), 1371–1379 (1995).
20. M. H. Macdougal, J. Geske, C. K. Lin, A. E. Bond, and P. D. Dapkus, "Low resistance intracavity-contacted oxide-aperture VCSEL's," IEEE Photonics Technol. Lett. **10**(1), 9–11 (1998).
21. Y. J. Yang, T. G. Dziura, T. Bardin, S. C. Wang, and R. Fernandez, "Continuous wave single transverse mode vertical-cavity surface-emitting lasers fabricated by Helium implantation and zinc diffusion," Electron. Lett. **28**(3), 274–276 (1992).
22. I. Harrison, H. P. Ho, B. Tuck, M. Henini, and O. H. Hughes, "Zn diffusion-induced disorder in AlAs/GaAs superlatttices," Semicond. Sci. Technol. **4**(10), 841–846 (1989).
23. J.-W. Shi, C.-C. Chen, Y.-S. Wu, S.-H. Guol, C. Kuo, and Y.-J. Yang, "High power and high-speed Zn-diffusion single fundamental-mode vertical cavity surface-emitting lasers at 850 nm wavelength," IEEE Photonics Technol. Lett. **20**(13), 1121–1123 (2008).
24. N. Suzuki, H. Hatakeyama, K. Fukatsu, T. Anan, K. Yashiki, and M. Tsuji, "25-Gbps operation of 1.1-μm-range InGaAs VCSELs for high-speed optical interconnections," in *Conference on Optical Fiber Communication* Conf. (Anaheim, CA, USA, 2006), paper OFA4.
25. W. Hofmann, N. H. Zhu, M. Ortsiefer, G. Bohm, J. Rosskopf, L. Chao, S. Zhang, M. Maute, and M.-C. Amann, "10-Gb/s data transmission using BCB passivated 1.55-/spl mu/m InGaAlAs-InP VCSELs," IEEE Photonics Technol. Lett. **18**(2), 424–426 (2006).
26. D. M. Kuchta, A. V. Rylyakov, F. E. Doany, C. L. Schow, J. E. Proesel, C. W. Baks, P. Westbergh, J. S. Gustavsson, and A. Larsson, "A 71-Gb/s NRZ modulated 850-nm VCSEL-based optical link," IEEE Photonics Technol. Lett. **27**(6), 577–580 (2015).
27. P. Moser, J. A. Lott, and D. Bimberg, "Energy efficiency of directly modulated oxide-confined high bit rate 850 nm VCSELs for optical interconnects," IEEE J. Sel. Top. Quantum Electron. **19**(4), 1702212 (2013).
28. S.-Y. Lin, Y.-C. Su, Y.-C. Li, H.-L. Wang, G.-C. Lin, S.-M. Chen, and G.-R. Lin, "10-Gbit/s direct modulation of a TO-56-can packed 600-μm long laser diode with 2% front-facet reflectance," Opt. Express **21**(21), 25197–25209 (2013).
29. K. Szczerba, P. Westbergh, E. Agrell, M. Karlsson, P. A. Andrekson, and A. Larsson, "Comparison of intersymbol interference power penalties for OOK and 4-PAM in short-range optical links," J. Lightwave Technol. **31**(22), 3525–3534 (2013).
30. F. Breyer, S. C. J. Lee, S. Randel, and N. Hanik, "Comparison of OOK and PAM-4 modulation for 10 Gbit/s transmission over up to 300 m polymer optical fiber," in *Conference on Optical Fiber Communication* (San Diego, CA, USA, 2008), paper OWB5.

Optics EXPRESS

31. J. Lavrencik, S. Varighese, A. Varghese, G. Landry, Y. Sun, R. Shubochkin, and K. Balemarthy, "100 Gbps PAM-4 Transmission over 100m OM4 and wideband fiber using 850nm VCSELs," in *Conference on European Conference and Exhibition on Optical Communication* (Dusseldorf, Germany, 2016), paper Th.1.C.5.
32. Y.-C. Chi, Y.-C. Li, H.-Y. Wang, P.-C. Peng, H.-H. Lu, and G.-R. Lin, "Optical 16-QAM-52-OFDM transmission at 4 Gbit/s by directly modulating a coherently injection-locked colorless laser diode," Opt. Express **20**(18), 20071–20077 (2012).
33. F. Karinou, L. Deng, R. R. Lopez, K. Prince, J. B. Jensen, and I. T. Monroy, "Performance comparison of 850-nm and 1550-nm VCSELs exploiting OOK, OFDM, and 4-PAM over SMF/MMF links for low-cost optical interconnects," Opt. Fiber Technol. **19**(3), 206–212 (2013).
34. R. Puerta, M. Agustin, L. Chorchos, J. Tonski, J.-R. Kropp, N. Ledentsov, V. A. Shchukin, N. N. Ledentsov, R. Henker, I. T. Monroy, J. J. V. Olmos, and J. P. Turkiewicz, "107.5 Gb/s 850 nm multi- and single-mode VCSEL transmission over 10 and 100 m of multi-mode fiber," in *Conference on Optical Fiber Communication* (Anaheim, CA, USA, 2016), paper Th5B.5.
35. I.-C. Lu, C.-C. Wei, H.-Y. Chen, K.-Z. Chen, C.-H. Huang, K.-L. Chi, J.-W. Shi, F.-I. Lai, D.-H. Hsieh, H.-C. Kuo, W. Lin, S.-W. Chiu, and J. Chen, "Very high bit-rate distance product using high-power single-mode 850-nm VCSEL with discrete multitone modulation formats through OM4 multimode fiber," IEEE J. Sel. Top. Quantum Electron. **21**(6), 444 (2015).
36. C. Kottke, C. Caspar, V. Jungnickel, R. Freund, M. Agustin, and N. Ledentsov, "High speed 160 Gb/s DMT VCSEL transmission using pre-equalization," in *Conference on Optical Fiber Communication* (Los Angeles, CA, USA, 2017), paper W4I.7.
37. P. Westbergh, J. S. Gustavsson, Å. Haglund, M. Skold, A. Joel, and A. Larsson, "High-speed, low-current-density 850 nm VCSELs," IEEE J. Sel. Top. Quantum Electron. **15**(3), 694–703 (2009).
38. E. Haglund, Å. Haglund, J. S. Gustavsson, B. Kögel, P. Westbergh, and A. Larsson, "Reducing the spectral width of high speed oxide confined VCSELs using an integrated mode filter," Proc. SPIE **8276**, 82760L (2012).
39. K.-L. Chi, Y.-X. Shi, X.-N. Chen, J. Chen, Y.-J. Yang, J.-R. Kropp, N. Ledentsov, Jr., M. Agustin, N. N. Ledentsov, G. Stepniak, J. P. Turkiewicz, and J.-W. Shi, "Single-mode 850-nm VCSELs for 54-Gb/s on-off keying transmission over 1-km multi-mode fiber," IEEE Photonics Technol. Lett. **28**(12), 1367–1370 (2016).
40. P. V. Mena, J. J. Morikuni, S. M. Kang, A. V. Harton, and K. W. Wyatt, "A simple rate-equation-based thermal VCSEL model," J. Lightwave Technol. **17**(5), 865–872 (1999).
41. A. N. Al-Omari and K. L. Lear, "VCSELs with a self-aligned contact and copper-plated heatsink," IEEE Photonics Technol. Lett. **17**(9), 1767–1769 (2005).
42. J. Piprek, T. Tröger, B. Schröter, J. Kolodzey, and C. S. Ih, "Thermal conductivity reduction in GaAs-AlAs distributed bragg reflectors," IEEE Photonics Technol. Lett. **10**(1), 81–83 (1998).
43. M.-C. Cheng, Y.-C. Chi, Y.-C. Li, C.-T. Tsai, and G.-R. Lin, "Suppressing the relaxation oscillation noise of injection-locked WRC-FPLD for directly modulated OFDM transmission," Opt. Express **22**(13), 15724–15736 (2014).
44. S. E. Hashemi, *Relative intensity noise (RIN) in high-speed VCSELs for short reach communication*, (Chalmers, 2012)
45. "Series G: Transmission systems and media, digital systems and networks," http://www.certificate.net/Portals/1/Standards/ITU/g-107.doc
46. E. K. Lau, X. Zhao, H.-K. Sung, D. Parekh, C. Chang-Hasnain, and M. C. Wu, "Strong optical injection-locked semiconductor lasers demonstrating > 100-GHz resonance frequencies and 80-GHz intrinsic bandwidths," Opt. Express **16**(9), 6609–6618 (2008).

1. Introduction

High-speed data centers and optical interconnects [1] rely strictly on developing ultrafast optical transmitters to solve the heavy data traffic induced from data switching/routing in central offices, and add/drop among remote nodes, and so on. To fulfill such demands standardized by IEEE P802.bs [2], the transmission capacity of laser diode modules have been up-scaled from 100 Gbit/s/module to 400Gbit/s/module for constructing cloud data centers based on the use of 8-channel vertical cavity surface emitting laser (VCSEL) array transmitter with 50 Gbit/s/channel [3]. At current stage, the set of directly modulated 850-nm multi-mode (MM) VCSELs and multi-mode fiber (MMF) link between racks in data centers has emerged as a cost-effective solution [4–6]. The well-known advantages of such a link include the efficient coupling with low power consumption [7], the high power conversion efficiency with low threshold condition [8,9], which makes the VCSEL an irreplaceable candidate for the aforementioned applications. However, the allowable transmission data rate or distance is still limited by both the direct modulation bandwidth, and the inevitable modal dispersion among different transverse mode occurring during the transmission in MMF [10]. Disregarding the severe modal dispersion in the commercially available MMF, the limitation on encoding bandwidth of the MM VCSEL is an important issue considered to be solved via

Optics EXPRESS

study of few-mode VCSELs currently. In view of previous works, the shrinkage of the emission aperture confined via oxidation has emerged as the simplest approach for obtaining quasi-single-mode or single-mode (SM) VCSEL transmitter [11–16].

Since 2004, Haglund, *et al.* have demonstrated a high-power SM VCSEL transmitter by narrowing the oxide-confined aperture size to 3 μm [16]. By utilizing a quasi-single-mode VCSEL with a similar aperture size of ~3 μm, Szczerba, *et al.* successfully implemented the PAM-4 transmission link at 25-Gbit/s over 500-m OM3 MMF in 2012 [12]. Apart from shrinking the aperture size via oxidation confinement, Tan *et al* designed a photonic crystal structure to achieve SM emission in the VCSEL transmitter for carrying 25-Gbit/s data over 1 km MMF in 2013 [17]. In 2014, Safaisini *et al.* integrated a mode filter generated with surface relief to realize a SM VCSEL transmitter for delivering 20-Gbit/s data through a 2-km-long MMF link [18]. Obviously, minimizing the diameter of oxide-confined aperture can increase the transverse mode spacing [19] and reduce the optical field area of the VCSEL to rule out the lasing of other high-order transverse modes, which is essential for supporting few-mode (FM) or even SM lasing in the VCSEL. Nonetheless, the differential resistance of the VCSEL would increase as the oxide-confined aperture reduces, which enlarges the voltage standing-wave ratio to suppress the modulation depth when directly encoding the data onto the SM VCSEL [20]. Such a drawback of the SM VCSEL can effectively be solved by introducing heavy zinc dopants into the top distributed Bragg reflector (DBR) mirror via diffusion, which can achieve good ohmic contact and avoid free-carrier absorption [21–23]. Moreover, the thick benzocyclobutene passivation layer with low capacitance was considered to replace the traditional SiO_2 passivation layer for improving the RC charging/discharging time [24] of the VCSEL [25].

For practical application, several studies of the VCSEL with various data formats for intra-data center links have been illustrated. Recently, Kuchta *et al.* used VCSEL to carry non-return-to-zero on-off-keying (NRZ-OOK) data at 71 Gbit/s over 7-m MMF [26]. A comparison of MM, FM and SM VCSELs on carrying NRZ-OOK data format for back-to-back (BtB) transmission was reported [27]. However, the low spectral usage efficiency of the NRZ-OOK makes the VCSEL require large modulation bandwidth for encoding [28]. To achieve the same data rate, 4-level pulse amplitude modulation (PAM-4) data is an alternative approach for decoding the VCSEL, since it only needs half of modulation bandwidth when comparing with NRZ-OOK data [29, 30]. In 2016, encoding PAM-4 onto an unpackaged VCSEL to achieve 100 Gbit/s over 100-m MMF with a pre-emphasis filter technology was proposed [31]. Therein the pre-emphasis filter is a digital filter embedded in the arbitrary waveform generator (AWG), which can pre-distort the transmitted signal to compensate the signal degradation during channel transmission for improving the transmission performance. To further exceed the data rate by maintaining the same encoding bandwidth, the quadrature amplitude modulation orthogonal frequency division multiplexing (QAM-OFDM) enables to provide the highest spectral usage efficiency when comparing with other data formats [32,33]. In 2016, Puerta *et al*. demonstrated a carrierless amplitude phase (CAP) transmission link at 107.5 Gbit/s by using an 850-nm multi-mode VCSEL over 10-m MMF [34]. Liu *et al.* demonstrated a zinc-diffused single-mode 850-nm VCSEL to provide a modulation bandwidth of 12 GHz for achieving the discrete multi-tone algorithm (DMT) up to 50 Gbit/s [35]. In 2017, Kottke *et al.* demonstrated a DMT link over 500-m MMF at the rate up to 135 Gbit/s by using an 850nm VCSEL with the assistance of the Volterra based pre-equalizer [36]. However, the comparison among MM, FM and SM VCSELs on carrying QAM-OFDM data for MMF transmission in the intra-data center has not been discussed previously yet.

In this work, the zinc-diffused VCSEL chips with MM, FM and SM output spectra at 850 nm are fabricated to demonstrate the 16-QAM OFDM data transmission over 100-m OM4-MMF. The basic characteristics including power-to-current-voltage (L-I-V) curve, differential resistance, small-signal analog modulation response, relative intensity noise (RIN) and the maximal allowable transmission capacity of the MM/FM/SM VCSEL chips are characterized

Optics EXPRESS

and compared with one another. For the practical application in data center, both the transmission performances under BtB and in 100-m-long OM4-MMF conditions are compared, and the key parameters including error vector magnitude (EVM), signal-to-noise ratio (SNR) and bit error ratio (BER) and receiving power penalty are determined and optimized in both cases.

2. Experimental setup and analyzing technique

2.1 Device fabrication

The 2-D and 3-D device structures of three MM/FM/SM VCSEL chips were illustrated in Fig. 1. The insets in the middle row present the near-infrared microscopic image of the oxide confined cross-section area on the top of the active region. For MM VCSEL chip, an n-type mirror containing 38 pairs of $Al_{0.15}Ga_{0.85}As/Al_{0.9}Ga_{0.1}As$ layers were grown to serve as the bottom DBR layer. The traditional MM VCSEL chip consists of an oxide-confined aperture of 11 μm, and 4 sets of strained $In_{0.15}Ga_{0.85}As/Al_{0.37}Ga_{0.63}As$ quantum wells with thickness of 3/6 nm for each layer are designed in the intrinsic active region. The oxide aperture size is exactly the same as the metal contact for the MM VCSEL chip. During the oxidation process, the scanning electron microscope is used to confirm the oxidation diameter and depth. Hence, the aperture underneath the metal edge can be precisely controlled. Finally, the 24 pairs of p-type $Al_{0.15}Ga_{0.85}As/Al_{0.9}Ga_{0.1}As$ layers were grown to complete the top DBR layer. In contrast, both FM and SM VCSEL chips exhibit 37 and 21 pairs of $Al_{0.9}Ga_{0.1}As/Al_{0.12}Ga_{0.88}As$ layers in the bottom and top DBR structures, and their intrinsic active region only consists of three strained $In_{0.08}Ga_{0.92}As$ quantum wells with well thickness of 5 nm. To achieve the few and single transverse mode operations, the designed oxide-confined apertures in the VCSEL must respectively reduce their diameters to 5 μm and 3 μm for the FM and SM VCSEL chips. Finally, a 500 Å thick p-type GaAs heavily doped with zinc-diffusion was employed as the contact layer in the top DBR. The parameters of the layer structures for three devices were compared in the Table 1.

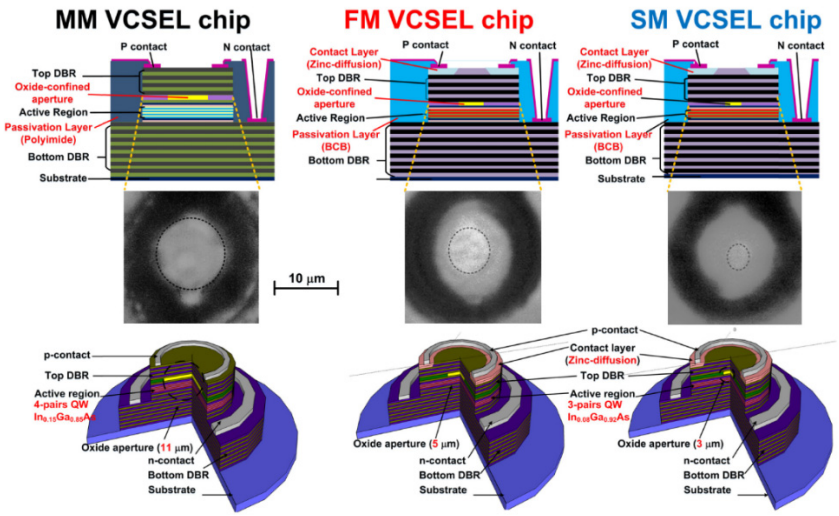

Fig. 1. The 2-D, 3-D -structures and microscopic image of oxide confined cross-section area of MM/FM/SM VCSEL chips.

In experiments, the MM VCSEL chip exhibits similar recipe with commercially available devices, which was fabricated to serve as a reference of commercial devices without zinc-diffusion process. The FM/SM VCSELs are designed with incorporating zinc-diffusion process to further reduce the parasitic resistance of the VCSEL. The zinc-diffusion and

Optics EXPRESS

passivation material may help to slightly improve the modulation bandwidth but will not affect the number of transverse modes to affect the data transmission capabilities. Based on previous simulation and experience, the QW and DBR design of the VCSEL chips would not affect the number of transverse modes in VCSEL chip significantly. Indeed, the alteration of DBR periods, passivation layer, zinc-diffusion and number of quantum wells could somewhat modify the modulation response. However, the modal dispersion related to the mode number predominates the transmission performance and the oxidation aperture size mainly controls the mode number. That is, even the layer structures of these VCSEL chips are slightly different, the comparison between mode number and its effect on the transmission distance still validates when dispersion play important role on the distortion of the transmitted data.

Table 1. Parameters for MM/FM/SM VCSEL chips

Parameters	MM	FM	SM
Aperture (μm)	11	5	3
Threshold current (mA)	1.7	0.22	0.18
Maximal optical power (mW)	8.67	2.22	0.88
Differential resistance (Ω)	30	112.5	215
η_{ed}	0.43	0.34	0.24
RMS spectral width (nm)	1.04	0.443	0
−3 dB bandwidth (GHz)	16 (@ $12I_{th}$)	21.2 (@ $20I_{th}$)	21.5 (@ $20I_{th}$)
RIN (dBc/Hz)	noise background	−163.1 (@ $20I_{th}$)	−163.05(@ $20I_{th}$)
RIN peak (GHz)	-	15.75(@ $20I_{th}$)	16.47(@ $20I_{th}$)
Quantum Well	4 $In_{0.15}Ga_{0.85}As$	3 $In_{0.8}Ga_{0.92}As$	
Zinc-diffusion	×	✓	
DBR Layers	$Al_{0.15}Ga_{0.85}As$/ $Al_{0.9}Ga_{0.1}As$	$Al_{0.9}Ga_{0.1}As$ / $Al_{0.12}Ga_{0.88}As$	
Top DBR #	24 pairs	21 pairs	
Bottom DBR #	38 pairs	37 pairs	
Passivation (RF permittivity)	Polyimide (3.2)	BCB (2.6)	

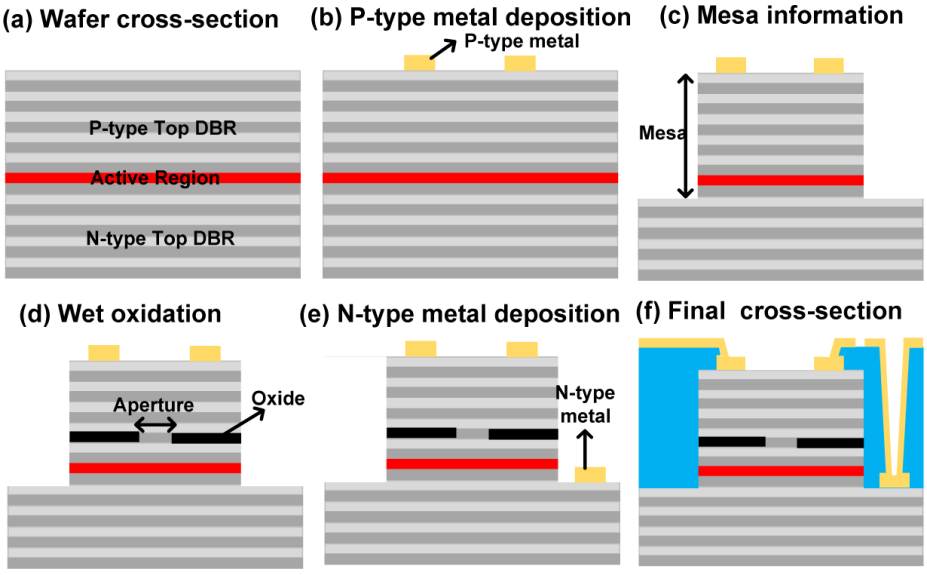

Fig. 2. The fabrication process of the VCSEL chip. (a) Epitaxial device structure on wafer. (b) p-type metal deposition and pattering. (c) Cylindrical mesa etching. (d) wet-oxidation for cross-section area confinement. (e) n-type metallic contact deposition. (f) Hole formation for contact pad finalization.

Optics EXPRESS

The process flow of our MM/FM/SM VCSEL chips is shown in Fig. 2. Firstly, the Ti/Pt/Au metallic films are deposited as the p-type contact by electron beam evaporation. Then, a mesa with outer diameter of 18 μm is defined by dry etching process using the inductively-coupled plasma reactive ion etching (RIE) equipment. The optical emission aperture is created and controlled by oxidation with hot water vapor and nitrogen at 420°C in the furnace. Afterwards, the Au/Ge/Ni/Au metallic films are then deposited as the n-type contact through e-beam evaporation followed by planarization with polyimide. The via holes are then opened using RIE. Finally, the Ti/Au metals are deposited as the contact pad of VCSEL chip to finish the device process, as shown in Fig. 2(f). Note that the process of the few-mode (FM) and single-mode (SM) VCSEL chips is similar except the additional zinc-diffusion process, different oxidation depths, and passivation materials. The step of the zinc-diffusion is carried out before the process of the p-type metal evaporation. In the zinc-diffused region of the top DBR, the induced disordering of $Al_{0.9}Ga_{0.1}As$ and $Al_{0.12}Ga_{0.88}As$ can improve the continuity of bandgap and index of refraction to avoid the free carrier absorption. In this way, the resistance of the top DBR is effectively reduced, which is beneficial to the modulation bandwidth for FM and SM VCSEL chips. To improve the response and isolation, a benzocyclobutene is employed to replace polyimide as the passivation layer, which provide lower parasitic capacitance for better modulation performance of the FM and SM VCSEL chips.

2.2 Device testing

The experimental setup of the directly 16-QAM OFDM encoded 850-nm MM/FM/SM VCSEL chips for 100-m OM4-MMF transmission is shown in Fig. 3. A homemade probe station was established during experiments, which consists of a ground-signal-ground (GSG) probe (GGB, 40A-GSG-100-DP) with analog −3dB bandwidth of 40 GHz, a microwave cable (HUBER + SUHNER, M8041-61616), a segment of lensed fiber (SHUODA) and its probe holder (EverBeing), a 100-m-long OM4-MMF (POFC, MMF50002PB) and a water-cooled heat sink (Deryun, DFC-4PT03) were used for testing the VCSEL chips. To stabilize the output performance, the temperature of all VCSEL chips was precisely controlled at 22°C. A 65-GHz bias-tee (Anritsu, V250) was employed for combining the DC bias current with transmitted 16-QAM OFDM. For data transmission test, the electrical 16-QAM OFDM data was generated by a homemade MATLAB program. At beginning, a serial pseudo-random bit sequence (PRBS) data stream with a length of 2^{15}-1 was mapped into QAM symbols, and the symbols were parallel distributed into 197 OFDM subcarriers in frequency domain. Subsequently, the 16-QAM OFDM waveform pattern in time domain was formed through the inverse Fourier transform (IFFT) with an FFT size of 512. To up-scale the carrier frequency of the 16-QAM OFDM, the electrical 16-QAM OFDM data was exported into an arbitrary waveform generator (AWG, Keysight M8195A) with a sampling rate of 65 GS/s. Afterwards, the 16-QAM OFDM data stream covering a bandwidth of up to 25 GHz is delivered from the AWG for directly encoding the VCSEL chips at a raw data rate of up to 100 Gbit/s.

Optics EXPRESS

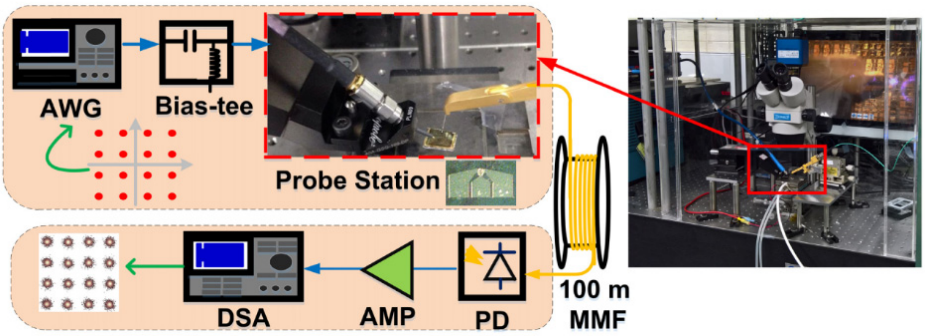

Fig. 3. The experimental setup of propose VCSEL chips based on 16-QAM OFDM over 100-m MMF.

To optimize the encoding response, the MM, FM and SM VCSEL chips were biased at 19.5 mA ($11.5I_{th}$), 4.5 mA ($20.4I_{th}$) and 3 mA ($13.9I_{th}$), respectively. For intra-data center application, the optical data was coupled into a lensed fiber connecting with a 100-m OM4-MMF cable. After propagating through 100-m MMF, a high-speed photodetector (PD, New Focus 1484-A-50) with −3dB bandwidth of 22 GHz was employed to convert the 16-QAM OFDM from optical to electrical data stream. To compensate the power attenuation induced during MMF transmission, a 35-GHz wideband microwave amplifier (AMP, Picosecond 5882) with a power gain of 16 dB and a noise figure of 6 dB was employed before waveform extraction. Then, the amplified 16-QAM OFDM data was sent into a digital serial analyzer (DSA, Tektronix DPO77002SX) with a sampling rate of 100 GS/s. After grabbing the waveform in time domain, the 16-QAM OFDM data was resampled and decoded by an off-line homemade MATLAB program to analyze the constellation plot, ratio, SNR, and BER of the received data.

3. Results and discussions

3.1 Basic characteristics of MM/FM/SM VCSEL chips

The lasing spectra, power-current-voltage (L-I-V) responses, and biased dependent differential resistances of the MM/FM/SM VCSEL chips at wavelengths around 850 nm are shown in Fig. 4, in which the black, red and blue colors represent the MM, FM and SM VCSEL chips, respectively. Note that the MM VCSEL chip exhibits more than 15 transverse modes at wavelengths ranging from 856 nm to 863 nm. The FM VCSEL chip has only 3-4 transverse modes within 838-840 nm, and the peak mode was centered at wavelength of 839.44 nm. In contrast, the SM VCSEL exhibits a single transverse mode located at 841.86 nm. The labels "X" shown in the Fig. 4(a) are employed to describe the optical signal-to-noise ratios (OSNR) for MM, FM, and SM VCSEL chips. The MM, FM, and SM VCSEL chips reveal the OSNRs of 28.8, 37.42, and 37.54 dB at the bias current of $10I_{th}$, $15I_{th}$, and $15I_{th}$ mA, respectively. The RMS spectral width is employed to describe the intensity distribution for the output optical spectrum of the VCSEL chip in the revised manuscript. In principle, the RMS spectral width ($\Delta\lambda_{RMS}$) of the VCSEL chip can be expressed as [37, 38]:

$$\Delta\lambda_{RMS} = \sqrt{\left[\sum_{i=1}^{n} P_i\left(\lambda_i - \sum_{i=1}^{n} P_i\lambda_i \Big/ \sum_{i=1}^{n} P_i\right)^2\right] \Big/ \sum_{i=1}^{n} P_i}, \quad (1)$$

where P_i and λ_i denote the peak power and wavelength of ith modes of the VCSEL chip, respectively. The RMS spectral widths of 1.02, 0.443, and 0 nm are calculated according to the Eq. (1) for MM, FM, and SM VCSEL chips, respectively. As the RMS spectral width of the SM VCSEL chip obtained from the Eq. (1) is 0 nm, the full width at half maximum

Optics EXPRESS

(FWHM) of the transverse mode of 0.026 nm is also quoted for the transverse mode of the SM VCSEL chip. In comparison, the RMS spectral width of 0.52 nm for FM VCSEL chip was previously reported [39], and our proposed FM VCSEL chip can provide the reduced RMS spectral width of 0.443 nm. Due to the high OSNR characteristic, our proposed SM VCSEL chip only exhibits a small FWHM as its RMS spectral width is 0 nm.

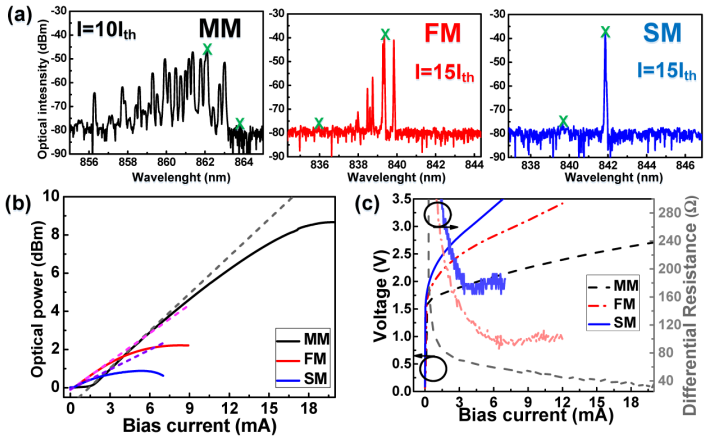

Fig. 4. The (a) optical spectra, (b) L-I curve, (c) V-I curve and corresponding differential resistance of MM, FM and SM VCSELs.

In viewing the L-I curves, the VCSEL with smaller oxide-confined aperture ensures higher injection current density to induce lower threshold current [14]. In comparison, the SM VCSEL chip with an aperture size of only 3 μm exhibits a threshold current as small as 0.18 mA, which is significantly lower than those of 0.22 mA and 1.7 mA for the FM and MM VCSEL chips, respectively. To obtain the differential quantum efficiency (η_{ed}) of the VCSEL chip, the dP_{out}/dI_{bias} slope of the whole L-I curve is calculated, and only the value obtained from the linear region at bias beyond the threshold current of the VCSEL chip are employed for further calculation afterwards. As extracted from Fig. 4(b), the differential quantum efficiencies defined as $\eta_{ed} = (q/h\nu)(dP_{out}/dI_{bias})$ for the MM, FM and SM VCSEL chips are calculated as 0.43, 0.34 and 0.24, respectively. Theoretically, the SM VCSEL chip should provide the highest emission quantum efficiency due to its rigorous control on the overlap between gain and waveguide regions. Nevertheless, the heat dissipation became a serious problem in the FM/SM VCSEL devices with smaller aperture, which cause the optical power saturation behavior at smaller bias currents. Such a phenomenon not only degrades the differential quantum efficiency of emission via non-radiative process, but also shrink the dynamic range for linear modulation to increase the differential resistance and to limit the maximal output power at same bias. As the VCSEL chip with larger oxide coverage easily accumulates heat to induce Auger effect, the SM VCSEL chip exhibits the fastest output power saturation trend at the lowest bias current as compared to the MM and the FM VCSEL chips. As a result, the large-area oxidation confinement inevitably decreases the modulation depth of the VCSEL chip. In contrast, the MM VCSEL chip exhibits the highest L-I slope to provide the highest optical power of 8.67 mW among three VCSEL chips. When three VCSEL chips are operated at the same bias current before output saturation, the one with smaller oxide-confined aperture represents the higher injection current density and exhibits the larger differential resistance. The electrical reflection coefficient (Γ), electrical return loss (RL), and electrical voltage standing wave ratio (VSWR) are defined as following: $\Gamma = (Z_i - Z_0)/(Z_i + Z_0)$, $RL = 10\log(\Gamma)^2$ and $VSWR = (1 + \Gamma)/(1-\Gamma)$ with Z_i and Z_0 denoting impedance of the VCSEL and all the components used for driving the VCSEL chip in experiments, including microwave probe, coaxial cables, and bias-tee. Among the MM/FM/SM VCSEL

Optics EXPRESS

chips, the MM VCSEL chip exhibits the lowest differential resistance of 30 Ω with an electrical return loss of −12.04 dB and the electrical VSWR of 1.67 at an optimized bias current of 19.5 mA (equivalent to $11.7I_{th}$). The smallest differential resistance of 112.5 Ω and the electrical VSWR of 2.25 with corresponding electrical return loss of −8.3 dB are obtained for the FM VCSEL chip operated at 4.5 mA (equivalent to $20I_{th}$), whereas the SM VCSEL chip has its differential resistance as high as 215 Ω with the smallest electrical return loss of −4.1 dB and the electrical VSWR of 4.3 at optimized bias of 2.5 mA (equivalent to $14I_{th}$). When the compliance voltage enlarges beyond 2.5 V for these VCSEL chips, the differential resistances of FM and MM VCSEL chips show a fluctuation trend because of the instability of zinc atom.

Next, the power-to-frequency throughput responses of MM, FM and SM VCSEL chips under small-signal analog modulation are illustrated in Fig. 5(a), in which the 0 dB defines the normalized optical response at the first measuring point. At the same bias current ratio of $5I_{th}$, the MM VCSEL chip exhibits a relaxation oscillation peak at frequency of 7.6 GHz and a −3dB analog modulation bandwidth of 11.2 GHz. In practice, the largest direct modulation bandwidth can be enhanced to 16 GHz by enlarging the bias current ratio up to $12I_{th}$; however, the overdriven operation beyond $12I_{th}$ induces the thermal roller-over effect [40] to limit the output power with reduced radiative emission efficiency. In discussion of the improvement on thermal, in the previous literatures, the heat transfer improvement [41] and the AlAs/GaAs DBR [42] were introduced to release the thermal effect. The method for the improvement will be considered in the future work. By increasing the bias current ratio from $5I_{th}$ to $10I_{th}$, the analog modulation responses of the FM and SM VCSEL chips can enlarge their −3dB bandwidth from 15.7 to 19.5 GHz and from 15.2 to 18.5 GHz, respectively. Further enlarging the bias current to $20I_{th}$ also extends the −3dB modulation bandwidths to 21.2 GHz for the FM VCSEL and 21.5 GHz for the SM VCSEL chips, respectively. The capability of such a bandwidth enhancement originates from the superior conductivity of the p-type top-DBR mirror, as the zinc-diffusion process effectively reduces the top-DBR layer resistance to provide improved modulation bandwidth for the FM and SM VCSEL chips. In detail, the smaller oxide-confined aperture induces lower capacitance to improve the modulation bandwidth of the SM VCSEL chip more than that of the FM VCSEL chip at the same bias current ratio. In addition, the optimization on zinc-diffusion recipe will be considered to further improve the resistance of the VCSEL chip.

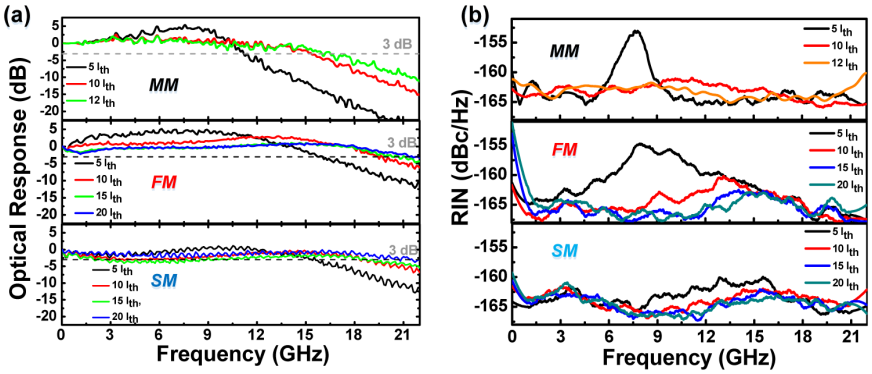

Fig. 5. (a) The small-signal frequency responses of MM, FM and SM VCSEL chips at different bias current ratios; (b) The comparison in dependence of the applied bias current on RIN response.

The noise figure of the VCSEL is another important parameter that could degrade the SNR of the data directly encoded onto the VCSEL carrier. Therefore, the bias-dependent RIN spectra of the MM/FM/SM VCSEL chips are compared in Fig. 5(b), which are measured by

Optics EXPRESS

using a lightwave signal analyzer (HP, 71300C). Note that the broadband peak noise observed in RIN spectrum is correlated with the relaxation oscillation feature of the VCSEL [43]. For the MM VCSEL chip, its RIN peak can upshift from 7.6 to 11.1 GHz with corresponding power level reduced from −153.33 to −161.17 dBc/Hz, respectively, by increasing the bias current from 8.5 mA ($5I_{th}$) to 17 mA ($10I_{th}$). Increasing the bias current up to 20.4 mA (12 I_{th}) effectively makes the RIN power level merged into the noise background, in which the shot/thermal noises of the PD and the intensity noise trans-impedance amplifiers are contributed to the noise level. For the FM/SM VCSEL chip, their RIN peaks are upshifted from 7.92/12.9 to 15.75/16.47 GHz such that the noise power levels are suppressed from −154.4/-160.5 to −163.1/-163.05 dBc/Hz, respectively. With decreasing oxide-confined aperture size, the reduced volume increases the optical photon density S_b owing to the gain confinement in the VCSEL chip. In principle, the relaxation frequencies f_r are directly proportional to the optical photon density S_b, and the damping factor γ is a function of the relaxation frequency with $\gamma \propto f_r^{\,2}$ [44]. As the SM VCSEL chip is made with a small oxide-confined aperture, the relatively high relaxation oscillation frequency and large damping factor result in low RIN power level when comparing with the MM VCSEL chips at the same bias current ratio of $5I_{th}$. At even larger biased condition, such an excellent noise suppression feature can be observed in the VCSELs with few- or single mode, which guarantees the enhancement on the SNR of delivered data after receiving by the PD at remote node.

3.2 BtB-16-QAM OFDM transmission

After BtB transmission, the MM/FM/SM VCSEL chips provide different allowable encoding bandwidths at their optimized bias currents. At their maximal data rates of transmission, the subcarrier SNR response of three VCSEL chip directly encoded by 16-QAM OFDM data with the same peak-to-peak amplitude of 1 V are shown in Fig. 6 for comparison. For OFDM data analysis, the forward error correction (FEC) criterion is introduced, which is a correction process that pre-embeds the FEC codes into the data stream to be delivered and uses it to correct the received data stream at the receiving end. According to the ITU-T Recommendation G.975.1 [45], the BER of the received signal can be greatly corrected to less than 1×10^{-15} for an input data stream with a BER of 3.8×10^{-3}. This is achieved by employing two interleaved extended Bose-Chaudhuri-Hocquengham (1020,988) super FEC codes with an erasure algorithm. Without any signal processing or pre-emphasis, the SM VCSEL chip biased at 1.5 mA can carry 16-QAM OFDM data covering a bandwidth of 17 GHz, and the average SNR of 16.18 dB and BER of 1.5×10^{-3} are obtained at a raw data rate of 68 Gbit/s. Because of the enhancement on analog modulation bandwidth, enlarging the bias current to 2.5 mA can further improve the average SNR and BER to 17.95 dB and 1.5×10^{-4}, respectively.

Optics EXPRESS

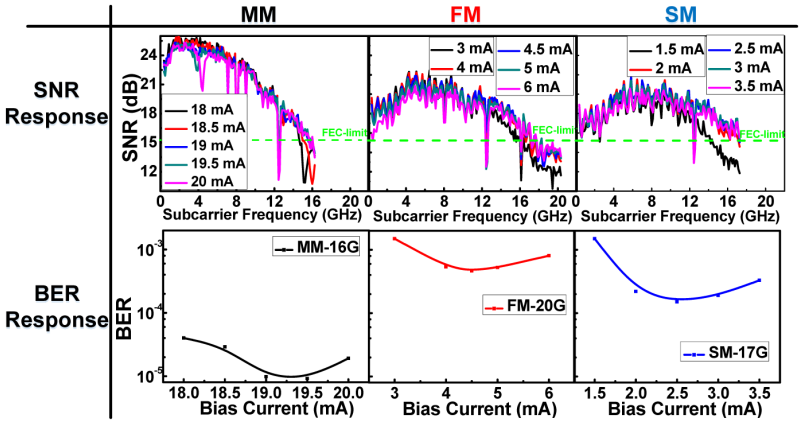

Fig. 6. The SNR and BER responses of MM/FM/SM VCSEL chips carried and BtB transmitted 16/20/17-GHz 16-QAM OFDM data.

However, the overdriven VCSEL at bias beyond 3.5 mA conversely shows slight degradation with the SNR decreased by 0.5 dB and the BER increased by two times. These results from the inevitably induced modulation roll-off effect of the SM VCSEL under over-bias condition, which significantly deteriorate the SNR of data carried by the low-frequency OFDM subcarriers [46]. Therefore, the SM VCSEL chip biased at optimized current of 2.5 mA ($13.9I_{th}$) makes a compromise between the enhanced modulation bandwidth and the gradually enlarged roll-off on the modulation throughput. Similarly, optimizing the bias currents of the MM and FM VCSEL chips at 19.5 ($11.5I_{th}$) and 4.5 mA ($20.4I_{th}$) allow the delivery of 16-QAM OFDM data with corresponding bandwidths of 16 GHz and 20 GHz at raw data rates of 64 and 80 Gbit/s, respectively. The related average SNRs of 19.5 and 17.17 dB and BERs of 9.17×10^{-6} and 4.65×10^{-4} are also observed for the received data from FM and MM VCSEL chips, respectively. Although the used OFDM data bandwidths are different for three VCSEL chips, they exhibit similar trend on the bias current dependent optimization as dominated by the modulation roll-off degradation. In comparison with the FM and SM VCSEL chips, the MM VCSEL chip with its differential resistance closest to 50 Ω results in the lowest return loss, which somewhat allows the encoding of data with the largest peak-to-peak voltage. In spite of the impedance matching, the rapid decay on the throughput within finite bandwidth still predominates the overall modulation performance. That is why the MM VCSEL chip requires the highest bias current even with the highest modulation depth among all VCSELs.

To perform a fair comparison at same raw data rate of 80 Gbit/s, Fig. 7 illustrates the RF spectra, SNRs responses and corresponding constellation plots of the 16-QAM OFDM data delivered by the MM, FM and SM VCSEL chips after BtB transmission. The electrical signal before encoding the VCSEL chip with corresponding parameters are also presented as a reference. The electrical signal exhibits the clearest constellation plot with the highest average SNR of 22.58 dB among all cases. To achieve successful 80-Gbit/s encoding, three VCSEL chips are individually operated at their optimized bias currents (19.5/4.5/2.5 mA for the MM/FM/SM VCSEL chips). When comparing with the FM and SM VCSEL chips, the MM VCSEL chip carrying 80-Gbit/s data shows the largely declined throughput with a significant delay at frequency >14 GHz. In addition, the relaxation oscillation related RIN peak at 21.4 GHz is observed outside the OFDM encoding bandwidth of 20 GHz. In contrast, the SM VCSEL chips exhibit a flat throughput in the RF spectrum of the received OFDM data due to its wide and even modulation response within −3dB bandwidth. Although the three VCSEL chips can ensure the FEC qualified performance at 80-Gbit/s BtB transmission, the MM VCSEL chip carried data provides the lowest SNR of 15.9 dB with the largest BER of 2 ×

Optics EXPRESS

10^{-3} and the highest EVM of 16% among all cases. Undoubtedly, the FM and SM VCSEL chips reveal the higher SNRs of 17.2 and 17 dB to give the larger BERs/EVMs of 4.6 × 10^{-4}/13.9% and 6.6 × 10^{-4}/14.3%, respectively.

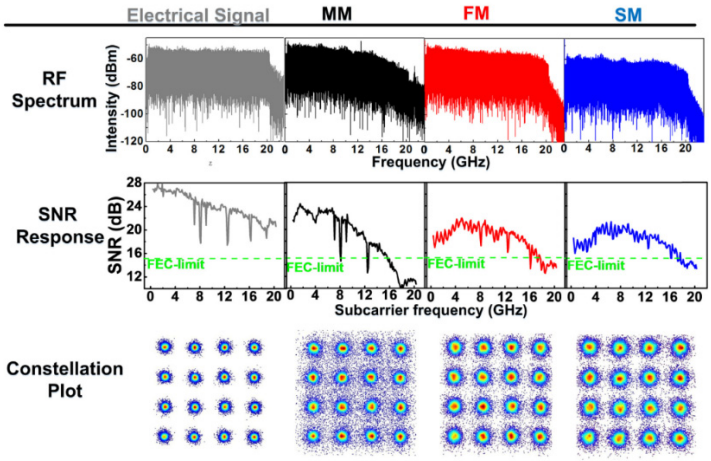

Fig. 7. The RF spectra, subcarrier SNRs responses and constellation plots of the electrical, MM, FM, and SM VCSEL chips carried 80 Gbit/s 16-QAM OFDM data after BtB transmission.

Note that the SM VCSEL show overall performance less comparable with the FM VCSEL chip, which is due to its relatively high differential resistance and large interior heat accumulation. As a result, the SM VCSEL shows the larger VSWR and the higher return loss to give a lower modulation throughput. Furthermore, the severer power saturation of caused by Auger effect under heat accumulation in the SM VCSEL somewhat degrades the linear modulation response, which distorts the OFDM waveform in the time domain and results in spectral reshaping in frequency domain to give a less stabilized output as compared to the FM VCSEL. Such a result can also be verified from the decoded constellation plots. The degraded uneven throughput of the MM-VCSEL delivered data also reveals the blurriest constellation plot. After performing the ultimate encoding performance with adequate pre-leveling on the 16-QAM-OFDM data, Fig. 8(a) illustrates the received BERs of BtB transmitted data streams carried by three VCSEL chips all achieve their highest allowable data rate at related bandwidths. For the MM VCSEL chip, the maximal allowable OFDM data bandwidth is 21 GHz at raw data rate of 84 Gbit/s, and the related BER, SNR and EVM are 3.5 × 10^{-3}, 15.3 dB and 17.1%, respectively.

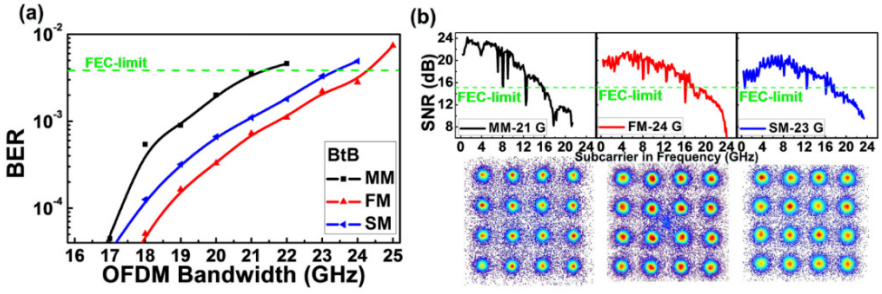

Fig. 8. (a) The BtB transmitted BERs of the MM, FM, SM VCSEL chips carried 16-QAM OFDM data at different bandwidths; (b) The SNRs responses of MM/FM/SM VCSEL chip carried 84/96/92-Gbit/s 16-QAM OFDM data and related constellation plots.

Optics EXPRESS

The SNR responses and related constellation plots of three VCSEL chips encoded by 16-QAM OFDM data at maximal transmission capacities are shown in Fig. 8(b). With the use of SM and FM VCSEL chips, the significant progress on enlarging the maximal allowable bandwidths to 23 and 24 GHz with data rate of 92 and 96 Gbit/s has been realized, enabling the receiving of OFDM data with corresponding BER/SNR/EVM of 2.8×10^{-3}/15.5dB/16.7% and 3.3×10^{-3}/15.4dB/17%, respectively. Note that the FM VCSEL chip carrying 96-Gbit/s data spectrum shows dramatic attenuation at subcarrier frequency >23.5 GHz is due to the PD with a limited cutoff frequency at 22 GHz. As elucidated, the difference on transmission capacity among three VCSEL chips is mainly attributed to the combined effect by differential resistance, heat accumulation, −3dB modulation bandwidth, and modulation throughput declination. The performance of the MM VCSEL chip is dominated by its small modulation bandwidth and declined throughput. The SM VCSEL suffers from insufficient thermal dissipation in the active region due to its larger oxidation layer as compared to the FM VCSEL. It is no wonder that the FM VCSEL with larger output power and stronger modulation throughput than others can offer the higher OFDM bandwidth available for transmission. In addition, if the ion-implanted layer could provide better heat dissipation, it is an alternative for confining the current aperture.

3.3 100-m OM4-MMF-16-QAM OFDM transmission

For data center applications, the transmission distance is lengthened to 100 m by connecting the lensed fiber patchcord with an OM4-MMF cable. By setting the raw data rate at 80 Gbit/s initially, the RF spectra, SNR responses and related constellation plots of the 100-m OM4-MMF transmitted QAM data carried by MM, FM and SM VCSEL chips are displayed in Fig. 9. Except for the SM-VCSEL carried data, the transmitted data in the other two cases would concurrently suffer from the optical modal dispersion and microwave power fading to distort its waveform. As expected, the constellation plots of the MM/FM/SM VCSEL delivered 80-Gbit/s data become blurred with the EVMs degraded from 16.0%/13.9%/14.3% to 27.9%/17.8%/18.3%, the average SNRs reduced from 15.9/17.2/16.9 to 11.4/15.0/14.8 dB, and the BERs increased from 2.2×10^{-3}/4.6×10^{-4}/6.6×10^{-4} to 3.6×10^{-2}/4.4×10^{-3}/5.4×10^{-3}. In fact, the dispersion induced delay and distortion cannot be easily distinguished as the off-line extracted QAM-OFDM data stream in time domain is a relatively complicated waveform. In the on-off-keying PRBS-NRZ data stream with a TTL-like bit shape, the data waveform distortion induced by modal/chromatic dispersion can be easily distinguished from the original data waveform in time domain. Typically, the rising/falling time and the duty-cycle of the bit shape would be enlarged due to the deviated modal velocity induced propagation delay among the transverse modes. However, such a sub-nanosecond shape distortion is relatively difficult to be monitored in the QAM-OFDM data stream with a complicated waveform shape. The only way to check the dispersion induced distortion in a QAM-OFDM data waveform is to compare the SNR spectral responses of the received QAM-OFDM data streams, as which could suffer from different scales of modal/chromatic dispersion when delivered by different transverse modes and OFDM subcarriers to cause a power attenuation, spectral reshaping as well as SNR degradation in the frequency domain.

Optics EXPRESS

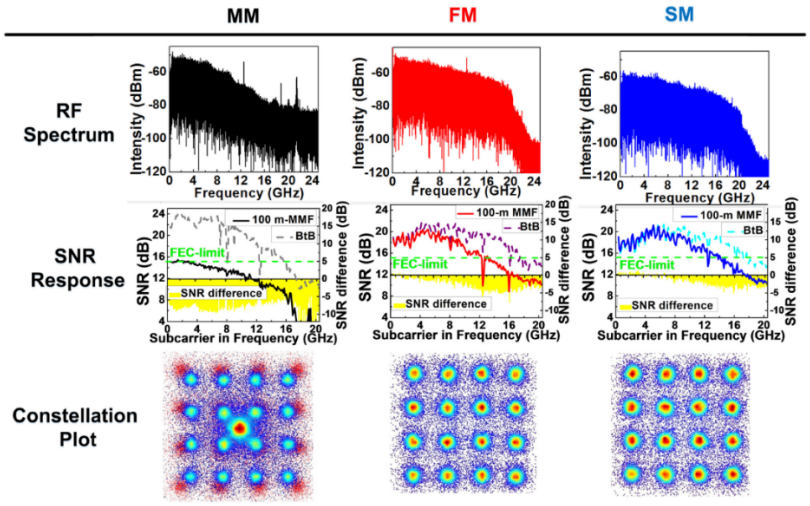

Fig. 9. The RF spectra, SNRs responses and constellation plots of the 100-m MMF transmitted 80-Gbit/s data carried by the MM, FM and SM VCSEL chips.

When comparing the BtB and MMF transmitted OFDM data, the constant power attenuation caused by propagation loss can be ruled out as it only results in an equivalent down offset on the SNR spectrum. Obviously, the declined subcarrier SNR degradation is not caused by the optical power attenuation but originates from the modal/chromatic dispersion induced RF fading effect. The QAM data carried by OFDM subcarrier at higher frequency would suffer from the larger shape distortion in time domain and higher SNR degradation in frequency domain. To compare, the SNR difference before and after 100-m OM4-MMF transmitted data are shown as the yellow bar chart in the middle column of Fig. 9. For MM and FM VCSEL chips, the modal dispersion dominate the waveform distortion in time domain and SNR degradation in frequency domain which induced the larger degradations of 4.5 and 2.2 dB on SNR. For the SM VCSEL chip, the single transverse mode rules out the modal dispersion effect during MMF transmission. Only the chromatic dispersion induced distortion and degradation is left with the delivered QAM-OFDM data stream. As a result, the SM VCSEL chip reveals a lowest SNR degradation of 2.1 dB compared with MM and FM VCSEL chips.

To improve the average SNR of the 100-m MMF transmitted data, the pre-leveled QAM-OFDM data that slightly sacrifices the low-frequency SNR to compensate the high-frequency SNR degradation is employed. Figure 10 compares the constellation plots, subcarrier SNRs, and received BERs of the MM/FM/SM-VCSEL carrying 64/80/80-Gbit/s data without and with OFDM subcarrier pre-leveling. In view of the 80-Gbit/s OFDM data carried by the MM VCSEL, most of the subcarrier SNR falls below the FEC criterion regardless of the pre-leveling or not. For a practical application, the allowable OFDM data bandwidth of the MM VCSEL chip is decreased to 16 GHz with corresponding raw data rate of 64 Gbit/s. With an OFDM pre-leveling slope of 0.4 dB/GHz, the BER and SNR are respectively observed as 3.3×10^{-3} and 15.4 dB, which meet the FEC required BER of 3.8×10^{-3} and SNR of 15.2 dB. For the FM-VCSEL carrying 80-Gibt/s data with subcarrier power pre-leveling at a slope of 0.3 dB/GHz, the BER and SNR are improved to 3.7×10^{-3} and 15.2 dB, respectively. Over pre-leveling with a slope beyond 0.4 dB/GHz excessively sacrifices the low-frequency SNR without favoring the high-frequency SNR. Note that the SM VCSEL chip also allows 80-Gbit/s 16-QAM OFDM transmission in 100-m OM4-MMF with a pre-leveling at a slope of 0.2 dB/GHz, which achieves BER of 3.5×10^{-3} and SNR of 15.3 dB that are better than those of the FM VCSEL. In particular, the optimized pre-leveling slope of QAM-OFDM data for the SM VCSEL chip is much lower than those required for FM and MM VCSEL chips, as the

Optics EXPRESS

SM VCSEL carrying QAM-OFDM data does not suffer from serious modal dispersion during MMF transmission.

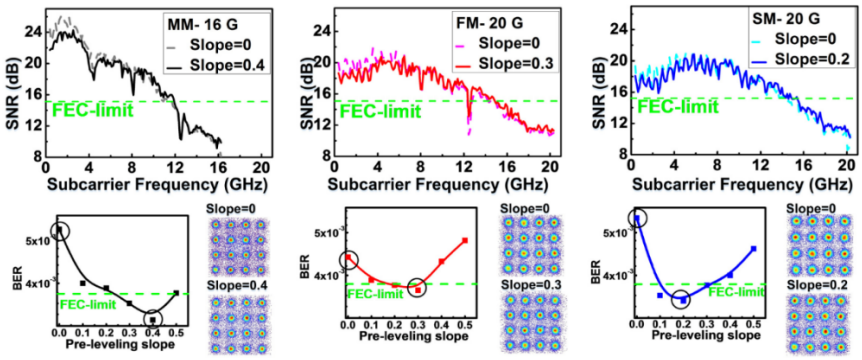

Fig. 10. The SNRs, constellation plots and BERs of the 100-m OM4-MMF transmitted 64/80/80-Gbit/s data carried by the MM/FM/SM VCSEL chip before and after pre-leveling.

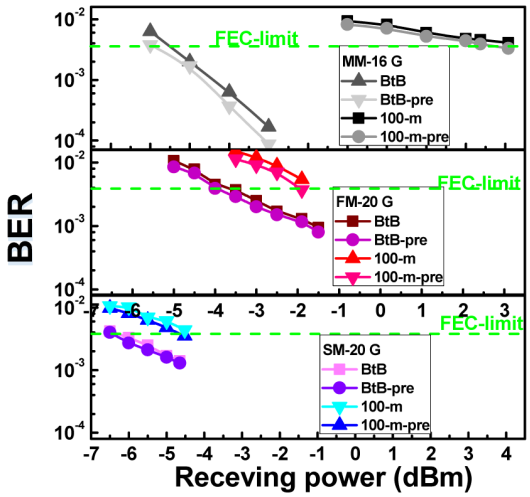

Fig. 11. BER versus receiving power of the MM/FM/SM VCSEL chip output with and without pre-leveling under BtB and 100-m OM4-MMF transmissions.

In more detail, the receiving power sensitivity of the MM/FM/SM VCSEL chips carried 64/80/80-Gbit/s 16-QAM OFDM data are compared in Fig. 11. The receiving power dependent BERs for all cases without and with pre-leveling are analyzed before and after 100-m MMF transmissions. No matter the OFDM data with and without pre-leveling, the MM-VCSEL carrying 64-Gbit/s data suffers from serious modal dispersion to show the highest power penalty of 9 and 8.5 dB before and after 100-m OM4-MMF transmissions, respectively. Without OFDM pre-leveling, the receiving power sensitivities of 80-Gbit/s data carried by FM and SM VCSEL chips before 100-m OM4-MMF transmission are −3.7 and −6.4 dBm, which are slightly increased to −1.5 and −4.3 dBm with power penalties of 2.2 and 2.1 dB, respectively, after propagating over 100-m OM4-MMF. Experimental results reveal that the SM VCSEL chip exhibits the lowest power penalty among three VCSEL chips due to its modal-dispersion-free transmission in the OM4-MMF. With utilizing the pre-leveling technique, the receiving power penalties before and after 100-m MMF transmissions can be efficiently suppressed to 2 and 1.8 dB for the FM- and SM-VCSEL carrying 80-Gbit/s data. These results have already declared the trade-off and comparability between FM and SM

Optics EXPRESS

VCSELs for their future usage on transmitting the high-spectral-density QAM-OFDM data formats in data centers.

4. Conclusion

The parametric comparisons of MM, FM and SM VCSEL chips at wavelength around 850 nm on their performance for carrying the pre-leveled 16-QAM OFDM data for BtB and 100-m OM4 MMF transmissions are performed. The MM/FM/SM VCSEL chips provide 15/3/1 transverse modes with corresponding aperture sizes of 11/5/3 μm to result in respective threshold currents of 1.7/0.22/0.18 mA. The MM VCSEL chip exhibits the highest differential quantum efficiency to provide the highest optical power of 8.67 mW and the lowest return loss of −12.04 dB. Nevertheless, the MM VCSEL provides the slowest modulation response among all devices in addition to its largest throughput and highest SNR. In contrast, the zinc-diffusion process provides the improved modulation bandwidths of 22 and 23 GHz for the FM and SM VCSEL chips, respectively, as compared to the MM VCSEL chip at the same bias current ratio. As compared to the MM and the FM VCSEL chips, the SM VCSEL chip has the highest differential resistance of 215 Ω to result in a return loss as high as −4.1 dB. The smallest aperture of the SM VCSEL chip not only provides the larger differential resistance but also induces the optical power saturation and Auger effect, which leads to the fastest output saturation trend at the lowest bias current. The SM VCSEL chip still exhibits the highest relaxation oscillation frequency and the largest damping factor that result in the lowest RIN power level.

The difference on transmission capacity in BtB transmission among three VCSEL chips is dominated by the combination of differential resistance, heat accumulation, −3dB modulation bandwidth, and modulation throughput declination. Among them, the MM VCSEL exhibits the lowest transmission capacity of 84-Gbit/s due to its small modulation bandwidth of 16 GHz and reduced throughput. The FM VCSEL chip with larger output power and stronger modulation throughput enables to carry the highest data rate of 96-Gbit/s 16-QAM OFDM data. In contrast, the SM VCSEL chip exhibits a comparable −3dB modulation bandwidth, and its transmission capacity at 92-Gbit/s is limited by the high differential resistance and induced Auger effect from heat accumulation. After transmitting over a 100-m OM4 MMF link, the MM VCSEL chip carried 16-QAM OFDM data experiences the most serious modal dispersion to decrease its maximal allowable data rate to 64-Gbit/s with BER and SNR of 3.3 $\times 10^{-3}$ and 15.4 dB, respectively. To meet the FEC criterion, a receiving power penalty of 8.5 dB is observed for the MM VCSEL chip. Although the FM VCSEL chip exhibits stronger modulation throughput, it carried 16-QAM OFDM data suffers from more modal dispersion than the SM VCSEL chip carried one after 100-m OM4 MMF transmission, which achieves a data rate of 80-Gbit/s with a power penalty of 2.08 dB. The characteristic of modal dispersion free makes the SM VCSEL chip exhibit the smallest data-rate degradation during transmission in OM4 MMF when comparing with other VCSEL chips. As a result, the SM VCSEL chip supports 80-Gbit/s data rate with BER and SNR 3.5 $\times 10^{-3}$ and 15.3 dB, respectively, and a receiving power penalty of only 1.8 dB is obtained after 100-m OM4 MMF transmission. This work declares the ability of MM/FM/SM VCSEL chips for high-speed intra-data center application, in which the SM VCSEL chip reveals the best performance as compared to other competitors. The optimization of the on zinc-diffusion recipe will be considered to further improve the thermal and resistance for SM VCSEL chip in the future.

Funding

Ministry of Science and Technology, Taiwan (MOST 104-2221-E-002-117-MY3, MOST 103-2221-E-002-042-MY3, MOST 103-2218-E-002-017-MY3, MOST 104-2218-E-005-004-).